Pharmacology and Clinical Pharmacy Research
Volume 10 No. 2 August 2025
ISSN:2527-7322 | e-ISSN: 2614-0020
doi: 10.15416/pcpr.v10i2.60233

Comprehensive In Silico Analysis of Bioactive Compounds from *P. Piloselloides* Leaves as Xanthine Oxidase Inhibitors

Masira S. C. Sinuhaji[1], Husnul Havid[1], Ysrafil Ysrafil[2], Francisca D. Alexandra[2]*

[1]Medical Education, Faculty of Medicine, Palangka Raya University, Palangka Raya
[2]Department of Pharmacotherapy, Faculty of Medicine, Palangka Raya University, Palangka Raya

Abstract

This study aimed to evaluate the potential of bioactive compounds from *P. piloselloides* leaves as xanthine oxidase (XO) inhibitors through an in silico approach. Methods included molecular docking and molecular dynamics simulations to identify the binding affinity of test compounds to XO. Among 59 screened compounds, 3 compounds (2,6,10,14,18,22-Tetracosahexaene, 6-Hydroxymethaqualone, and β-Sitosterol acetate) exhibited the lowest binding energy in comparison to the control, Allopurinol, with key residue contributions from GLU 802, ARG 880, and THR 1010. Molecular dynamics simulations confirmed the interaction stability, with β-Sitosterol acetate showing the lowest total binding free energy (-46.23 ± 0.66 kcal/mol). ADMET predictions revealed promising pharmacokinetic profiles for these compounds. This study highlights *P. piloselloides* as a promising source of novel XO inhibitors, with further validation required through in vitro and in vivo experiments.

Key words: gout, xanthine oxidase, *P. piloselloides*, in silico, molecular docking, molecular dynamics

Corresponding author: Francisca Diana Alexandra. Department of Pharmacotherapy, Faculty of Medicine, Palangka Raya University, Palangka Raya. Email: francisca.alexandra07@gmail.com
Received: 23 December 2024 **Revised**: 24 June 2025 **Published:** 01 August 2025.

Introduction

Gout is an increasingly prevalent variant of inflammatory arthritis, affecting more than 1% of the adult population in the United States, with a significantly higher prevalence in men, exhibiting an incidence rate 2 to 6 times greater than that observed in women[1]. The necessity to address gout arises from its correlation with numerous significant comorbid conditions, including hypertension, chronic kidney disease, obesity, diabetes mellitus, and cardiovascular disorders[2,3]. This pathology is primarily caused by elevated serum uric acid concentrations, which can trigger inflammation and acute arthralgia; furthermore, if left untreated, it has the potential to result in irreversible joint damage and systemic sequelae, including nephropathy[1,3]. The urgency of this concern is further underscored by the possibility of acute gout progressing into chronic gouty arthritis, which can exacerbate systemic health issues and significantly impair overall quality of life[3].

Bioactive compounds present in fruits and vegetables have been demonstrated to possess antioxidant, anti-inflammatory, and additionally anti-lipid characteristics. The consequent advantages of these constituents are substantial for public health[4]. Numerous studies have highlighted the presence of phytochemicals, including flavonoids, phenolic acids, and terpenoids, which have been shown to reduce uric acid concentrations and facilitate the dissolution of urate crystals, offering a natural alternative to traditional therapeutic interventions with reduced incidence of side effects[5,6].

Ethanol extracts and corresponding fractions derived from *P. piloselloides* have been identified to contain anthraquinones, flavonoids, terpenoids, steroids, saponins, phenolic compounds, and reducing sugars. The presence of these phytochemicals plays a crucial role in the manifestation of the plant's antibacterial and anti-inflammatory properties, as evidenced by significant inhibition of bacterial proliferation and reduced inflammatory responses in controlled experimental models[7].

Flavonoids, such as amentoflavone, have exhibited effectiveness in mitigating gouty arthritis through the inhibition of the NLRP3/ASC/Caspase-1 signaling pathway, which is integral to the inflammatory processes implicated in the pathophysiology of gout[8]. Similarly, flavonoids and phenolic acids play a critical role in modulating inflammation associated with gouty arthritis by suppressing signaling pathways such as NOD-like receptors, with a particular focus on the NRLP3/ASC/CASP1/IL1B axis[9]. Additionally, diterpenoids and triterpenoids have demonstrated significant efficacy in alleviating gouty arthritis and enhancing uric acid excretion, surpassing certain traditional uricosuric pharmacological agents within experimental research paradigms[10]. Phenolic compounds, flavonoids, and terpenoids have demonstrated efficacy in alleviating acute gouty arthritis manifestations through the modulation of various therapeutic pathways, including macrophage polarization and the NLRP3 inflammasome[11]. These phytochemicals, derived from natural sources, present an appealing alternative to traditional therapeutic approaches, with the potential to lower uric acid concentrations and facilitate the dissolution of monosodium urate crystals, thereby effectively mitigating hyperuricemia and gout[5].

Nevertheless, despite advancements in the investigation of gout and xanthine oxidase, the specific effects and mechanisms associated with *P. piloselloides* in relation to this disease remain inadequately explored. A more comprehensive understanding of these mechanisms can be achieved through the

application of molecular docking techniques. Furthermore, molecular dynamics should be considered, as this methodology is widely utilized in drug discovery processes for multifaceted conditions such as gout.

Molecular docking represents an advanced computational methodology that investigates interactions between ligand molecules, such as drugs, and their corresponding protein target receptors. This methodology is capable of validating the observed interactions between compounds derived from *P. piloselloides* leaves and the crucial enzyme xanthine oxidase, while simultaneously examining residue interactions and binding affinity[12]. Furthermore, to evaluate the equilibrium and adaptability of the intricate interactions between the investigational substance P. piloselloides and the utilized XO protein, molecular dynamics simulations are employed.

Therefore, this study aims to elucidate the impacts and mechanisms associated with the bioactive compounds of *P. piloselloides* on xanthine oxidase through the integration of molecular docking and molecular dynamics methodologies. A schematic representation of the research workflow is illustrated in Figure 1.

Method

Screening of bioactive compounds from P. piloselloides

All compounds derived from *P. piloselloides* were extracted from relevant scientific articles, where gas chromatography-mass spectrometry (GC-MS) analysis of aqueous and methanolic extracts from *P. piloselloides* leaves revealed 59 distinct bioactive compounds[13]. These compounds were screened using five parameters: molecular weight (< 500 Daltons), number of hydrogen-bond acceptors (< 10), number of hydrogen-bond donors (< 5), LogP (< 5), and molar refractivity (40-130)14–16. This methodology aims to ensure that the selected compounds meet ideal pharmacokinetic parameters. The screening process utilized tools and databases, including SwissADME (*http://www.swissadme.ch/index.php*) and SCFBIO-IITD (*http://www.scfbio-iitd.res.in/software/drugdesign/lipinski.jsp*).

Molecular docking

The crystal structure of XO, determined by x-ray diffraction at a resolution of 1.60 Å, was downloaded from the RSCB Protein Data Bank with PDB ID: 3NVW (*https://www.rcsb.org/*) (Figure 2). In 3NVW, GUN (guanine) was used to define the binding site, and chain C was separated from the native ligand prior to docking using Discovery Studio Visualizer software. The 3D structures of the test compounds were downloaded from the PubChem database (*https://pubchem.ncbi.nlm.nih.gov/*). Energy minimization was then performed using Chem3D software with MM2 force field parameters. The protein was prepared by removing water molecules and unnecessary residues, adding polar hydrogen atoms, and assigning Kollman charges using AutoDockTools to obtain the protein in .pdbqt format[17].

For docking, a grid box was set up to encompass the active site of XO. The grid box was centered at X = 38.017, Y = 20.172, Z = 18.698 with dimensions of 40 Å × 40 Å × 40 Å and a spacing of 0.375 Å. The search algorithm was configured to generate 100 GA runs, and binding energy calculations were performed using the Lamarckian Genetic Algorithm. Other parameters were kept at their default values. The docking mode with the lowest binding energy and the highest frequency percentage was selected to analyze the complex conformations. The outcomes were represented in 2D and 3D structures*18,19*.

ADMET Predictions

ADMET (Absorption, Distribution, Metabolism, Excretion, and Toxicity) analysis was conducted to evaluate the pharmacokinetic profile and toxicity potential of bioactive compounds from *P. piloselloides* to determine their therapeutic efficacy and success rate. This approach utilized web-based platforms including pkCSM (*http://biosig.unimelb.edu.au/pkcsm/prediction*), SwissADME (*http://www.swissadme.ch/index.php*), and admetSAR (*https://lmmd.ecust.edu.cn/admetsar3/index.php*) to predict the pharmacokinetic aspects of the compounds using in silico data[20].

Molecular Dynamics

Molecular dynamics simulations were executed utilizing the OpenMM and AMBER force fields within the Google Colab environment. The complexes were solvated using the TIP3P water model, neutralized by adding Na+ and Cl- ions, and energy-minimized for 1000 steps. The temperature was maintained at a constant 310 K with a 2 fs timestep for a duration of 5 ns. Molecular dynamics trajectories were recorded every 10 ps. The stability of the protein-ligand complexes was analyzed based on root mean square deviation (RMSD), root mean square fluctuation (RMSF), and radius of gyration (RoG). In this study, molecular dynamics simulations were performed on the three best test compounds, which exhibited the lowest free energy (ΔG) and inhibition constant (Ki) values, to assess the stability of ligand-receptor interactions under physiological conditions over time[20].

Result and Discussion

P. piloselloides Compounds Pass Screening

A comprehensive screening of 59 compounds derived from *P. piloselloides* was conducted using advanced computational tools, particularly SwissADME and SCFBIO-IITD. Following a thorough evaluation of the resulting data, nine compounds from *P. piloselloides* were found to meet the five established screening criteria. These compounds include Allopurinol, 6-Hydroxymethaqualone, 2,6,10,14,18,22-Tetracosahexaene, Ergost-8(14)-en-3-ol, (3β)-, Stigmasterol, Stigmast-7-en-3-ol, (3β,5α,24s)-, Stigmastan-3,5,22-trien, 7-Dehydrodiosgenin 3-acetate, and β-Sitosterol acetate (Table 1). These identified compounds were subsequently subjected to molecular docking in the next phase of the study.

Orally active bioactive compounds should not exhibit more than one violation of Lipinski's Rule of Five. If a compound violates multiple parameters, its absorption through the gastrointestinal tract becomes problematic, leading to reduced bioavailability. Despite this observation, many drugs violate Lipinski's principles yet continue to demonstrate oral activity. Lipinski's Rule posits the potential of a compound to undergo passive diffusion. However, this principle becomes less applicable in cases where compounds act as substrates for transporters, thereby facilitating their active diffusion[14,21]. Consequently, additional assessments of pharmacokinetic characteristics are imperative to thoroughly investigate the ADMET parameters associated with the compounds under examination.

According to the findings of this analysis, pharmaceutical compounds that exhibit more than one violation of Lipinski's Rule should be contraindicated for oral administration. Nevertheless, various delivery modalities have been developed to ensure that therapeutic agents effectively reach their intended biological targets, including but not limited to intravenous, intramuscular, buccal, or rectal routes[22]. Additionally, nanoparticles can serve

ISSN:2527-7322 | e-ISSN: 2614-0020

as carriers, facilitating the efficient absorption of complex compounds and their subsequent entry into cellular environments to elicit biological responses at specific target sites[23].

Optimization procedures and frequency evaluations aimed at minimizing binding energy were performed using ChemDraw and Chem3D software applications to obtain the most stable molecular configurations. From this analysis, we successfully identified ligands that exhibited stable modeling with the lowest energy values (Table 2).

Method Validation

Method validation was conducted to evaluate the success of the docking method through a comparative analysis of co-crystal ligands and re-docked ligands. This procedure involved re-docking between native ligand and the pre-prepared protein[8]. Docking method validation was performed to determine the root mean square deviation (RMSD) value. RMSD serves as an indicator of pose or the similarity of coordinates between two atoms. The docking method is considered valid if the RMSD value is below 2 Å, as lower RMSD values indicate closer alignment between the re-docked native ligand and the crystallographically observed ligand[24]. The re-docking was performed using the same grid box and parameters as those applied to the test compounds. The grid box was centered at X = 38.017, Y = 20.172, Z = 18.698 with dimensions of 40 Å × 40 Å × 40 Å and a grid spacing of 0.375 Å. Based on the results of the re-docking, an RMSD value of 0.27 Å was obtained for chain C, indicating that the docking method used is valid. This validation ensures that the docking process for the test compounds, consisting of secondary metabolites from *P. piloselloides* with xanthine oxidase, can be performed (Figure 2).

Molecular Docking

The in silico molecular docking method was used to predict the interactions between two docked molecules, resulting in a bound model. Molecular docking has the capacity to predict interaction models between small molecules (ligands) and macromolecules (proteins) in a stable binding site. The success of docking results is evaluated based on Gibbs Free Binding Energy (ΔG) and the inhibition constant (Ki).

Nine compounds were docked with the target protein to verify the therapeutic potential of the compounds found in P. piloselloides. These compounds include Allopurinol, 6-Hydroxymethaqualone, 2,6,10,14,18,22-Tetracosahexaene, Ergost-8(14)-en-3-ol, (3β)-, Stigmasterol, Stigmast-7-en-3-ol, (3β,5α,24S)-, Stigmastan-3,5,22-trien, 7-Dehydrodiosgenin 3-acetate, and β-Sitosterol acetate.

It was demonstrated that all compounds could interact with the protein. Among them, 2,6,10,14,18,22-Tetracosahexaene exhibited the lowest docking score (ΔG = −9.13 kcal/mol) (Figure 5 and Table 3). Moreover, other compounds (6-Hydroxymethaqualone and β-Sitosterol acetate) demonstrated enhanced binding affinity relative to the reference compound (allopurinol). In addition, as illustrated in Table 3, a diverse array of interactions occurred between the compounds and the target binding site, encompassing hydrogen bonds, Van der Waals interactions, Pi-Pi Stacked/Pi–Pi T-Shaped interactions, Pi–Sigma interactions, unfavorable, and Alkyl/Pi–Alkyl interactions.

The molecular docking results of the bioactive compounds from P. piloselloides leaves showed variations in binding energy against xanthine oxidase (XO), with some test compounds exhibiting very strong affinities. The compound 2,6,10,14,18,22-Tetracosahexaene recorded the lowest binding energy of

-9.13 kcal/mol and an inhibition constant (Ki) of 0.20 µM, indicating highly stable interactions. Similar results were observed for 6-Hydroxymethaqualone (-8.96 kcal/mol, Ki 0.27 µM) and β-Sitosterol acetate (-8.20 kcal/mol, Ki 0.97 µM), all of which demonstrated strong potential as XO inhibitors. In comparison, standard ligands such as guanine (-7.01 kcal/mol, Ki 7.24 µM) and allopurinol (-6.43 kcal/mol, Ki 19.48 µM) exhibited higher energy values, further emphasizing the superior efficacy of certain test compounds as alternative inhibitors.

Molecular interaction analysis revealed that key residues such as GLU 802, ARG 880, and THR 1010 play crucial roles in forming hydrogen bonds with the ligands. For instance, 6-Hydroxymethaqualone and β-Sitosterol acetate demonstrated significant hydrogen interactions with these residues, thereby enhancing the stability of the ligand-protein complexes[25]. Additionally, non-covalent interactions such as Pi-Pi stacking and Pi-Alkyl interactions involving hydrophobic residues like PHE 1009 and LEU 873 also contribute to binding stability through van der Waals interactions. The presence of these interactions strengthens the ligand's affinity for the active site, highlighting an effective molecular design for optimal binding.

The role of water molecules in the binding site is also crucial in thermodynamic mechanisms. Water molecules displaced by the ligand result in significant entropy gains, which contribute to the stability of the complex[26]. This is particularly relevant for compounds such as 2,6,10,14,18,22-Tetracosahexaene, which can displace less stable water molecules, thereby enhancing binding efficiency. This study supports the theory that water molecules within the binding pocket, especially those with low stability, can significantly influence binding affinity and validates the importance of water distribution analysis in structure-based drug design[27].

Pharmacologically, these findings indicate that compounds such as 6-Hydroxymethaqualone and β-Sitosterol acetate have significant potential for development as XO inhibitors. Their superior efficacy in comparison to allopurinol presents a promising opportunity for use as alternative therapies in the treatment of gout or hyperuricemia. Considering their pharmacokinetic and toxicity profiles, these compounds could serve as the foundation for the development of next-generation XO inhibitors. Further optimization, such as through molecular dynamics simulations, could enhance the selectivity and binding affinity of these ligands toward XO[28].

ADMET Predictions

The prediction of ADMET characteristics (Absorption, Distribution, Metabolism, Excretion, and Toxicity) is a critical phase in the pharmacological development process. In this investigation, three advanced computational tools (pkCSM, SwissADME, and admetSAR) were utilized due to their high accuracy in assessing the pharmacokinetic and toxicological profiles of various agents and pharmaceutical compounds (see Tables 4 and 5). The results showed that the intestinal absorption of the investigational compounds consistently outperformed the reference standard (allopurinol). While all three investigational compounds exhibited enhanced Caco-2 cell permeability in comparison to the reference standard, allopurinol demonstrated greater transdermal permeability than the investigational compounds.

6-Hydroxymethaqualone and 2,6,10,14,18,22-Tetracosahexaene demonstrated greater potential to function as substrates for P-glycoprotein (P-gp) in comparison to the control compound.

ISSN:2527-7322 | e-ISSN: 2614-0020

Furthermore, in terms of P-gp inhibition, all three test compounds exhibited significantly higher effectiveness than the positive control. The Volume of Distribution at Steady-State (VDSs) was observed to be lower for 6-Hydroxymethaqualone and β-Sitosterol acetate compared to the control. Regarding Blood-Brain Barrier (BBB) permeability, all test compounds achieved performance levels at or above that of the positive control. Most test compounds were metabolized by CYP3A4, except for allopurinol. Conversely, 6-Hydroxymethaqualone was the only compound capable of inhibiting metabolism by CYP1A2, CYP2C19, and CYP2C9. In terms of total clearance, only 2,6,10,14,18,22-Tetracosahexaene surpassed the positive control, with values indicating the fastest excretion rate among the evaluated compounds.

Regarding toxicity, all examined compounds exhibited lower maximum tolerated doses in comparison to the positive control. In AMES testing, all compounds were classified as non-mutagenic, except for 6-Hydroxymethaqualone. Carcinogenic potential varied among the compounds; however, none were predicted to be hepatotoxic. In terms of tetrahymena pyriformis toxicity (TPT), most tested compounds demonstrated relatively higher toxicity in comparison to the positive control. Acute oral toxicity was generally lower than the positive control, with the exception of 6-Hydroxymethaqualone. Furthermore, the test compounds showed lower oral rat chronic toxicity values in comparison to the positive control, except for 6-Hydroxymethaqualone. However, under chronic exposure conditions, β-sitosterol acetate exhibited greater toxicity than the positive control.

Molecular dynamics

The equilibrium and dynamics of ligand-protein interactions were thoroughly examined utilizing molecular dynamics simulations conducted over a duration of 5 ns. This analysis assessed root mean square deviation (RMSD), root mean square fluctuation (RMSF), and radius of gyration (RoG). As shown in Figures 6a–d, the RMSD metrics for the ligand-protein complexes, including XO-6-Hydroxymethaqualone, XO-2,6,10,14,18,22-Tetracosahexaene, and XO-β-Sitosterol Acetate, exhibited variations but consistently remained below 2 Å, similar to the interactions observed in the control compound. These observations indicate relatively stable binding affinities.

According to Figure 6a, the root mean square deviation (RMSD) of the interaction between xanthine oxidase (XO) and Allopurinol showed an increase during the initial 2 ns, followed by stabilization up to 5 ns. In contrast, the equilibrium phase associated with the interaction between XO and 6-Hydroxymethaqualone occurred between 1 and 4 ns, followed by a marginal decrease extending to 5 ns. For the interaction involving XO and 2,6,10,14,18,22-Tetracosahexaene, equilibrium was achieved within the first 2 ns, marked by a stable increase until 3.5 ns, followed by a slight reduction thereafter. Similarly, the interaction between XO and β-Sitosterol Acetate exhibited noticeable fluctuations, reaching stabilization at approximately 3.5 ns.

Furthermore, consistent with the root mean square deviation (RMSD) findings, the root mean square fluctuation (RMSF) analysis revealed favorable variations in the three ligand-receptor complexes, with measurements ranging from 0.35 to 3.79 Å, indicating strong interactions. However, the 16th amino acid residue in the XO-2,6,10,14,18,22-Tetracosahexaene complex showed an increased RMSF value of 5.39 Å.

Nonetheless, this specific measurement did not significantly deviate from the established RMSF range of the positive control (0.37–5.15 Å). RMSF analysis also indicated that key residues such as ARG 880, GLU 802, and THR 1010, located in the active site of XO, exhibited low fluctuations when interacting with β-Sitosterol Acetate, suggesting that this compound can maintain stable interactions within the active pocket. In contrast, although stable, Allopurinol displayed relatively weaker interactions compared to the tested bioactive compounds, as reflected by its lower interaction energy contributions[25].

Next, the stability and compactness of the protein-ligand complexes were evaluated by examining the radius of gyration (RoG) values during molecular dynamics simulations. The RoG values for the best complexes, namely XO-6-Hydroxymethaqualone (27.46–27.85 Å), XO-2,6,10,14,18,22-Tetracosahexaene (27.53–28.08 Å), and XO-β-Sitosterol Acetate (27.50–28.13 Å), were compared with the control compound (Allopurinol), which showed a range of 27.46–28.01 Å. The consistent RoG values across all complexes indicate that the protein maintained its structural compactness without significant unfolding or distortion upon ligand association. Although minor expansions were observed in XO-2,6,10,14,18,22-Tetracosahexaene and XO-β-Sitosterol Acetate, these variations remained within acceptable limits, demonstrating typical dynamic behavior. These findings underscore the stable and compact characteristics of the protein-ligand interactions, highlighting the identified ligands as promising inhibitors with favorable structural integrity.

From an energy perspective, the analysis indicates that van der Waals interactions (VDWALLS) are the dominant component supporting complex stability. β-Sitosterol acetate recorded the highest van der Waals energy contribution of -58.72 ± 0.95 kcal/mol, followed by 2,6,10,14,18,22-Tetracosahexaene (-46.41 ± 1.65 kcal/mol), while Allopurinol exhibited a much lower value (-13.57 ± 1.33 kcal/mol). These values suggest that β-Sitosterol acetate has a superior ability to access and interact with hydrophobic residues within the active pocket of XO[26]. Conversely, the electrostatic energy (EEL) contribution for Allopurinol was higher compared to the other compounds, indicating a binding mechanism that relies more heavily on polar interactions.

The total binding free energy (ΔG total) indicates that β-Sitosterol acetate possesses the strongest binding affinity with a ΔG total value of -46.23 ± 0.66 kcal/mol. 2,6,10,14,18,22-Tetracosahexaene and 6-Hydroxymethaqualone recorded ΔG total values of -35.85 ± 1.60 kcal/mol and -33.04 ± 0.85 kcal/mol, respectively. In comparison, Allopurinol recorded a significantly lower ΔG total value of -7.44 ± 1.57 kcal/mol, indicating a much weaker binding affinity[28]. The superior performance of β-Sitosterol acetate is supported by its significant van der Waals energy contributions and stable interactions with key residues in the active site (Table 6).

These results confirm that β-Sitosterol acetate is a highly potent candidate as an XO inhibitor, exhibiting high complex stability and strong binding affinity compared to the positive control, Allopurinol. The MD simulation-based approach provides valuable insights into the binding mechanisms and can serve as a foundation for the development of more effective XO inhibitors. Further research is required to validate these findings through in vitro and in vivo experiments[29].

Conclusion

This study identified the potential of bioactive compounds from *P. piloselloides* leaves as

xanthine oxidase (XO) inhibitors using an in silico approach. Molecular docking revealed that 2,6,10,14,18,22-Tetracosahexaene, 6-Hydroxymethaqualone, and β-Sitosterol acetate exhibited better binding affinities compared to the control, Allopurinol, with key residue interactions involving GLU 802, ARG 880, and THR 1010. Furthermore, the analysis predicted that these compounds possess pharmacokinetic and toxicological profiles worth considering for future development. Molecular dynamics simulations corroborated these findings, with β-Sitosterol acetate demonstrating the best stability, with a ΔG total of -46.23 ± 0.66 kcal/mol. However, as a computational study, this work is limited by simplified protein flexibility and short simulation times. Future research should include in vitro and in vivo validation, extended simulations, and structure-activity studies to support these findings and guide drug development.

Acknowledgements
We gratefully thanks to Medical Study Program and Faculty of Medicine Palangka Raya University. Conceptualization, M.S.C.S, F.D.A, and Y.Y.; Data curation, M.S.C.S and F.D.A; Formal analysis, M.S.C.S. and H.H.; Funding acquisition, M.S.C.S and H.H.; Investigation, M.S.C.S. and Y.Y.; Methodology, M.S.C.S, F.D.A, and Y.Y.; Project administration, M.S.C.S. and H.H.; Resources, M.S.C.S., H.H., and Y.Y.; Software, M.S.C.S. and Y.Y; Supervision, F.D.A and Y.Y.; Validation, F.D.A, Y.Y., and M.S.C.S; Visualization, M.S.C.S; Writing—original draft preparation, M.S.C.S. and H.H.; writing— review and editing, F.D.A, M.S.C.S., and H.H.; All authors revised the manuscript into its final form and given the approval for submission.

Funding
None

Conflict of Interest
None declared

References

1. Nehal S, Hussain SA. Gout- from a primary care perspective. 2024;V(I):27–34.
2. Adolph R. The management of gout: Much has changed. Australian Family Physician. 2016;45(5):1–23.
3. Premanath M. Acute Gout – A Harbinger for More Serious Outcome. APIK Journal of Internal Medicine. 2022;10(1):3–7.
4. Noce A, Di Lauro M, Di Daniele F, Zaitseva AP, Marrone G, Borboni P, et al. Natural bioactive compounds useful in clinical management of metabolic syndrome. Nutrients. 2021;13(2):1–37.
5. Wu J, Alhamoud Y, Lv S, Feng F, Wang J. Beneficial properties and mechanisms of natural phytochemicals to combat and prevent hyperuricemia and gout. Trends in Food Science & Technology. 2023 Aug 1;138:355–69.
6. Frazaei MH, Nouri R, Arefnezhad R, Pour PM, Naseri M, Assar S. A Review of Medicinal Plants and Phytochemicals for the Management of Gout. Current Rheumatology Reviews. 2023 Oct 13;20(3):223–40.
7. Cheng D, Zhang Y, Gao D, Zhang H. Antibacterial and anti-inflammatory activities of extract and fractions from Pyrrosia petiolosa (Christ et Bar.) Ching. Journal of Ethnopharmacology. 2014 Sep 11;155(2):1300–5.
8. Zhang X, Liu Y, Deng G, Huang B, Kai G, chen K, et al. A Purified Biflavonoid Extract From Selaginella moellendorffii Alleviates Gout Arthritis via NLRP3/ASC/Caspase-1 Axis Suppression. Frontiers in Pharmacology. 2021 May 17;12:676297.
9. Xiao N, Qu J, He S, Huang P, Qiao Y, Li G, et al. Exploring the Therapeutic Composition and Mechanism of Jiang-

Suan-Chu-Bi Recipe on Gouty Arthritis Using an Integrated Approach Based on Chemical Profile, Network Pharmacology and Experimental Support Using Molecular Cell Biology. Frontiers in pharmacology. 2020;10.
10. Chen W Di, Zhao YL, Sun WJ, He YJ, Liu YP, Jin Q, et al. "Kidney Tea" and Its Bioactive Secondary Metabolites for Treatment of Gout. Journal of agricultural and food chemistry. 2020 Aug 26;68(34):9131–8.
11. Wang S, Liu W, Wei B, Wang A, Wang Y, Wang W, et al. Traditional herbal medicine: Therapeutic potential in acute gouty arthritis. Journal of Ethnopharmacology. 2024 Aug 10;330:118182.
12. Pinzi L, Rastelli G. Molecular Docking: Shifting Paradigms in Drug Discovery. International journal of molecular sciences. 2019 Sep 1;20(18).
13. Sul'ain MD, Zakaria F, Johan MF. Anti-proliferative effects of methanol and water extracts of Pyrrosia piloselloides on the hela human cervical carcinoma cell line. Asian Pacific Journal of Cancer Prevention. 2019;20(1):185–92.
14. Agoni C, Olotu FA, Ramharack P, Soliman ME. Druggability and drug-likeness concepts in drug design: are biomodelling and predictive tools having their say? Journal of molecular modeling. 2020 Jun 1;26(6).
15. Lipinski CA. Lead- and drug-like compounds: the rule-of-five revolution. Drug Discovery Today: Technologies. 2004 Dec 1;1(4):337–41.
16. Jayaram B, Singh T, Mukherjee G, Mathur A, Shekhar S, Shekhar V. Sanjeevini: a freely accessible web-server for target directed lead molecule discovery. BMC bioinformatics. 2012 Dec 13;13 Suppl 17(17):1–13.
17. Ballante F. Protein-Ligand Docking in Drug Design: Performance Assessment and Binding-Pose Selection. Methods in Molecular Biology. 2018;1824:67–88.
18. Pan Y, Lu Z, Li C, Qi R, Chang H, Han L, et al. Molecular Dockings and Molecular Dynamics Simulations Reveal the Potency of Different Inhibitors against Xanthine Oxidase. ACS Omega. 2021;6(17):11639–49.
19. Zhao J, Huang L, Sun C, Zhao D, Tang H. Studies on the structure-activity relationship and interaction mechanism of flavonoids and xanthine oxidase through enzyme kinetics, spectroscopy methods and molecular simulations. Food Chemistry. 2020;323(February):126807.
20. Syahputra D, Ysrafil Y, Alexandra FD, Praja RK, Fatmaria F, Pratika RA. Network pharmacology combined with molecular docking and molecular dynamics to verify the therapeutic potential of mung beans (Vigna radiata) against prostate cancer. Beni-Suef University Journal of Basic and Applied Sciences. 2024;13(1).
21. Pollastri MP. Overview on the Rule of Five. Current protocols in pharmacology. 2010 Jun;Chapter 9(SUPPL. 49).
22. Kim J, Jesus O De. Medication Routes of Administration. StatPearls. 2023 Aug 23;
23. Azman M, Sabri AH, Anjani QK, Mustaffa MF, Hamid KA. Intestinal Absorption Study: Challenges and Absorption Enhancement Strategies in Improving Oral Drug Delivery. Pharmaceuticals (Basel, Switzerland). 2022 Aug 1;15(8).
24. Alcaide E, Gao Z, Ke G, Li Y, Zhang L, Zheng H, et al. Uni-Mol Docking V2: Towards Realistic and Accurate Binding Pose Prediction. 2024 May 20;
25. Cao H, Hall J, Hille R. Substrate orientation and specificity in xanthine oxidase: crystal structures of the enzyme in complex with indole-3-acetaldehyde and guanine. Biochemistry. 2014 Jan 28;53(3):533–41.
26. Dong C, Montes M, Al-Sawai WM. Xanthine oxidoreductase inhibition - A

review of computational aspect. Journal of Theoretical and Computational Chemistry. 2020 Jun 1;19(4).
27. Zhang B, Dai X, Bao Z, Mao Q, Duan Y, Yang Y, et al. Targeting the subpocket in xanthine oxidase: Design, synthesis, and biological evaluation of 2-[4-alkoxy-3-(1H-tetrazol-1-yl) phenyl]-6-oxo-1,6-dihydropyrimidine-5-carboxylic acid derivatives. European journal of medicinal chemistry. 2019 Nov 1;181.
28. Kumar R, Joshi G, Kler H, Kalra S, Kaur M, Arya R. Toward an Understanding of Structural Insights of Xanthine and Aldehyde Oxidases: An Overview of their Inhibitors and Role in Various Diseases. Medicinal research reviews. 2018 Jul 1;38(4):1073–125.
29. Schwarz G. Molybdenum cofactor and human disease. Current opinion in chemical biology. 2016 Apr 1;31:179–87.

ISSN:2527-7322 | e-ISSN: 2614-0020

Table 1. Analysis of Lipinski's Rule of Five for Test Compounds

Compound	Molecular Formula	SwissADME			SCFBIO-IITD		Violation
		Molecular Weight	Number of HBA	Number of HBD	LogP	Molar Refraction	
Allopurinol	$C_5H_4N_4O$	136.11	3	2	-0.18	34.20	1
6-Hydroxymethaqualone	$C_{16}H_{14}N_2O_2$	266.29	3	1	3.41	78.86	0
2,6,10,14,18,22-Tetracosahexaene	$C_{30}H_{50}$	410.72	0	0	10.60	140.06	2
Ergost-8(14)-en-3-ol, (3β)-	$C_{28}H_{48}O$	400.68	1	1	-0.05	77.14	0
Stigmasterol	$C_{29}H_{48}O$	412.69	1	1	7.80	128.12	1
Stigmast-7-en-3-ol, (3β,5α,24S)-	$C_{29}H_{50}O$	414.71	1	1	-0.05	77.14	0
Stigmastan-3,5,22-trien	$C_{29}H_{46}$	394.68	0	0	8.60	126.63	1
7-Dehydrodiosgenin 3-acetate	$C_{29}H_{42}O_4$	454.64	4	0	6.20	127.22	1
β-Sitosterol acetate	$C_{31}H_{52}O_2$	456.74	2	0	-0.05	77.14	0

Table 2. 2D and 3D structure of test compounds modelling

No	Compound	2D Structure	3D Structure
1	Allopurinol	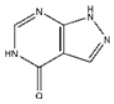	
2	6-Hydroxymethaqualone	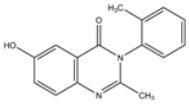	
3	2,6,10,14,18,22-Tetracosa-hexaene	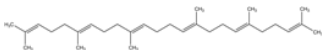	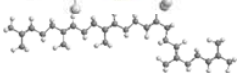
4	Ergost-8(14)-en-3-ol, (3β)-	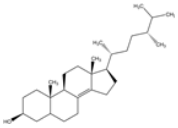	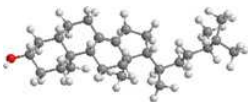
5	Stigmasterol	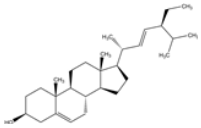	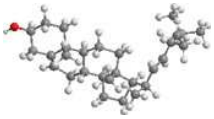
6	Stigmast-7-en-3-ol, (3β,5α,24S)-	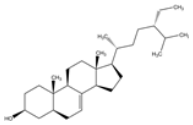	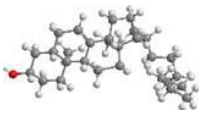
7	Stigmastan-3,5,22-trien	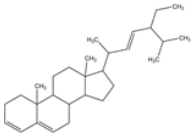	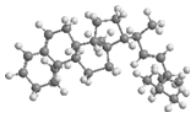

 ISSN:2527-7322 | e-ISSN: 2614-0020

8	7-Dehydrodiosgenin 3-acetate	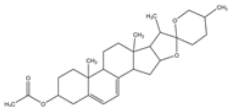	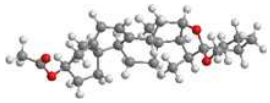
9	β-Sitosterol acetate	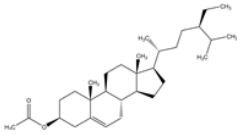	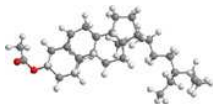

Table 3. Molecular Docking Results of the Native Ligand and Test Compounds Against XO

Ligand	Binding energy (ΔG) [kcal/mol]	Inhibition constant (Ki) [μM]	Hydrogen bond	Others bond	Shorter distance interaction (Å)
Guanine	-7,01	7,24 μM	GLU 802, THR 1010, ARG 880	ALA 910a, PRO 1076a, LEU 873a, LEU 1014a, SER 876a, SER 1008a, PHE 1009b, PHE 914b, VAL 1011b, ALA 1078e, ALA 1079e	1,78
Allopurinol	-6,43	19,48 μM	GLU 802, THR 1010, ARG 880	SER 876a, PHE 914a, LEU 1014a, LEU 873a, PRO 1076a, ALA 1078a, ALA 1079a, PHE 1009a, SER 1008a, VAL 1011d	1,74
6-Hydroxymethaqualone	-8,96	0,27 μM	GLU 802, ARG 880, SER 876, THR 1010, VAL 1011	ALA 1078a, PHE 649a, SER 1008a, PHE 1009b, PHE 914b, VAL 1011c, ALA 1079e, PRO 1076e, LEU 648e, LEU 873e, LEU 1014e, PHE 1013e	1,73
2,6,10,14,18,22-Tetracosahexaene	-9,13	0,20 μM	-	LYS 771a, ARG 880a, GLN 767a, GLU 1261a, GLY 799a, PHE 911a, ARG 912a, PHE 789a, SER 876a, THR 1010a, GLU 802a, PHE 914c, HIS 875e, PHE 649e, LEU 648e, LEU 873e, ALA 1079e, ALA 1078e, ALA 910e, PHE 1009e, VAL 1011e, LEU 1014e, PHE 1013e	2,87
Ergost-8(14)-en-3-ol, (3β)-	-3,25	4.160 μM	-	PHE 1013a, SER 876a, THR 1010a, ARG 880a, GLY 799a, PHE 911a, GLU 1261a, ARG 912a, GLY 913a, ALA 910a, ALA 1079a, GLU 802a, PRO 1076a, PHE 914c, VAL 1011e, LEU 873e, ALA 1078e, PHE 1009e, LEU 1014e, PHE 649e, LEU 648e	3,72

ISSN:2527-7322 | e-ISSN: 2614-0020

Stigmasterol	-6,00	40,16 µM	LYS 771	PHE 798a, GLY 799a, ARG 880a, GLU 802a, ASN 768a, THR 803a, SER 876a, THR 1010a, GLN 767a, SER 1080a, GLU 1261a, ARG 912a, GLY 913a, PHE 911a, ALA 910e, ALA 1079e, VAL 1011e, LEU 1014e, LEU 873e, PRO 1076e, PHE 1013e, LEU 648e, PHE 1009e, ALA 1078e, PHE 914e	2,51
Stigmast-7-en-3-ol, (3β,5α,24S)-	+2,60	-	-	ASN 768a, LYS 771a, SER 876a, THR 1010a, ARG 880a, LEU 873a, GLU 802a, SER 1075a, THR 803a, LEU 648e, VAL 1011e, PHE 1013e, ALA 1078e, ALA 1079e, PHE 914e, PHE 1009e, LEU 1014e, PRO 1076e, PHE 649e	2,91
Stigmastan-3,5,22-trien	-6,90	8,73 µM	-	ARG 880a, THR 1010a, SER 876a, PHE 1013a, THR 803a, GLU 802a, ASN 768a, SER 1080a, GLU 1261a, GLY 913a, ARG 912a, PHE 911a, GLY 799a, GLN 767a, PHE 914e, PHE 1009e, LYS 771e, LEU 648e, LEU 873e, LEU 1014e, VAL 1011e, PRO 1076e, ALA 1078e, ALA 910e, ALA 1079e	2,97
7-Dehydrodiosgenin 3-acetate	+28,62	-	-	GLU 1261a, PHE 1005a, ARG 880a, THR 1010a, THR 803a, GLU 802a, LYS 771a, SER 876a, PHE 1009d, LEU 1014d, LEU 873d, PHE 1009e, LEU 1014e, LEU 873e PRO 1076e, VAL 1011e, PHE 1013e, PHE 649e, LEU 648e, PHE 914e, ALA 1079e, ALA 1078e	2,24
β-Sitosterol acetate	-8,20	0,97 µM	LYS 771	SER 1080a, GLU 1261a, GLY 799a, ALA 1079a, ARG 880a, THR 1010a, SER 876a, PHE 649a, PHE 1013a, THR 803a, GLU 802a, PHE 914c, PHE 914e, VAL 1011e, PHE 1009e, LEU 648e, LEU 873e, LEU 1014e, PRO 1076e, ALA 910e, ALA 1078e	2,23

a = Van der walls, b = Pi-Pi Stacked/Pi-Pi T-shaped, c = Pi-Sigma, d = Unforable Donor-Donor, e = Alkyl/Pi-Alkyl

ISSN:2527-7322 | e-ISSN: 2614-0020

Table 4. Pharmacokinetic Properties of Selected Compounds from *P. piloselloides*

Compound	Absorption				Distribution				Metabolism							Excretion
	Human Intestinal Absorption (% Absorbed)	Caco2 cell permeability (%)	Caco2 permeability of the query molecule (%)	Log Kp (skin permeation) (cm/s)	P-gp substrate (%)	P-gp inhibitor (%)	VDss (human) (log L/Kg)	BBB Permeation (%)	CYP 2D6	CYP 3A4	CYP 1A2	CYP 2C19	CYP 2C9	CYP 2D6	CYP 3A4	Total Clearance (log ml/min/kg)
									Susbtrate		Inhibitor					
Allopurinol	79,511	73,12	20,5	-7,61	10,7	1,7	0,072	87,2	No	No	No	No	No	No	No	0,632
6-Hydroxymethaqualone	97,635	86,01	93,4	-6.40	26,7	16,5	0,007	87,2	No	Yes	Yes	Yes	Yes	No	No	0,577
2,6,10,14,18,22-Tetracosahexaene	89,002	96,19	86,3	-2,763	14	46,2	0,35	93,7	No	Yes	No	No	No	No	No	1,791
β-Sitosterol acetate	96,576	86,72	85,9	-2.05	6,5	46,5	0,066	94,4	No	Yes	No	No	No	No	No	0,551

ISSN:2527-7322 | e-ISSN: 2614-0020

Table 5. Toxicity Properties of Selected Compounds from *P. piloselloides*

Compound	Max. tolerated dose (human) (log mg/kg/day)	AMES toxicity	Carcinogens					Hepato-toxicity	Tetrahymena Pyriformis Toxicity pIGC50, ug/L		Acute oral toxicity log (1/ (mol/kg))		Oral Rat Acute Toxicity (LD50) (mol/kg)	Oral Rat Chronic Toxicity (log mg/kg_bw/day)
			Mouse carcinogenicity (+)	Mouse carcinogenicity (TD50)	Rat carcinogenicity (+)	Rat carcinogenicity (TD50)	Rodents carcinogenicity (+)		TPT (+)	TPT pIG50	AOT (+)	AOT (TD50)		
Allopurinol	0,957	No	47,8	36,96	47,2	23,99	51,8	No	36	40,76	41,5	33,59	1,922	1,713
6-Hydroxymethaqualone	-0,007	Yes	37,9	42,14	41,8	23,44	47	No	96	53,85	87,3	31,98	2,134	1,562
2,6,10,14,18,22-Tetracosahexaene	-0,533	No	47,9	46,49	37	20,69	43	No	97,3	91,05	3	11,68	1,893	0,911
β-Sitosterol acetate	-0,476	No	41,3	42,7	35,8	23,74	39,5	No	96,9	89,32	10	13,23	2,333	2,461

 ISSN:2527-7322 | e-ISSN: 2614-0020

Table 6. Free Energy Binding of Selected *P. piloselloides* Compounds During Molecular Dynamics Simulation

	Allopurinol	6-Hydroxymeth-aqualone	2,6,10,14,18,22-Tet-racosahexaene	β-Sitosterol acetate
Energy component	Average ± SEM	Average ± SEM	Average ± SEM	Average ± SEM
VDWALLS	-13.5651 ± 1.33	-34.5619 ± 0.90	-46.4093 ± 1.65	-58.7211 ± 0.95
EEL	-26.6820 ± 3.70	-24.9001 ± 1.35	0.2479 ± 0.54	1.2110 ± 1.58
EGB	35.1443 ± 3.06	31.1010 ± 1.18	17.0021 ± 0.64	18.4901 ± 1.90
ESURF	-2.3346 ± 0.14	-4.6793 ± 0.08	-6.6908 ± 0.21	-7.2095 ± 0.13
ΔG gas	-40.2471 ± 4.40	-59.4620 ± 1.57	-46.1614 ± 1.96	-57.5102 ± 2.31
ΔG solv	32.8097 ± 2.96	26.4218 ± 1.13	10.3113 ± 0.50	11.2806 ± 1.79
ΔTotal	-7.4375 ± 1.57	-33.0402 ± 0.85	-35.8501 ± 1.60	-46.2296 ± 0.66

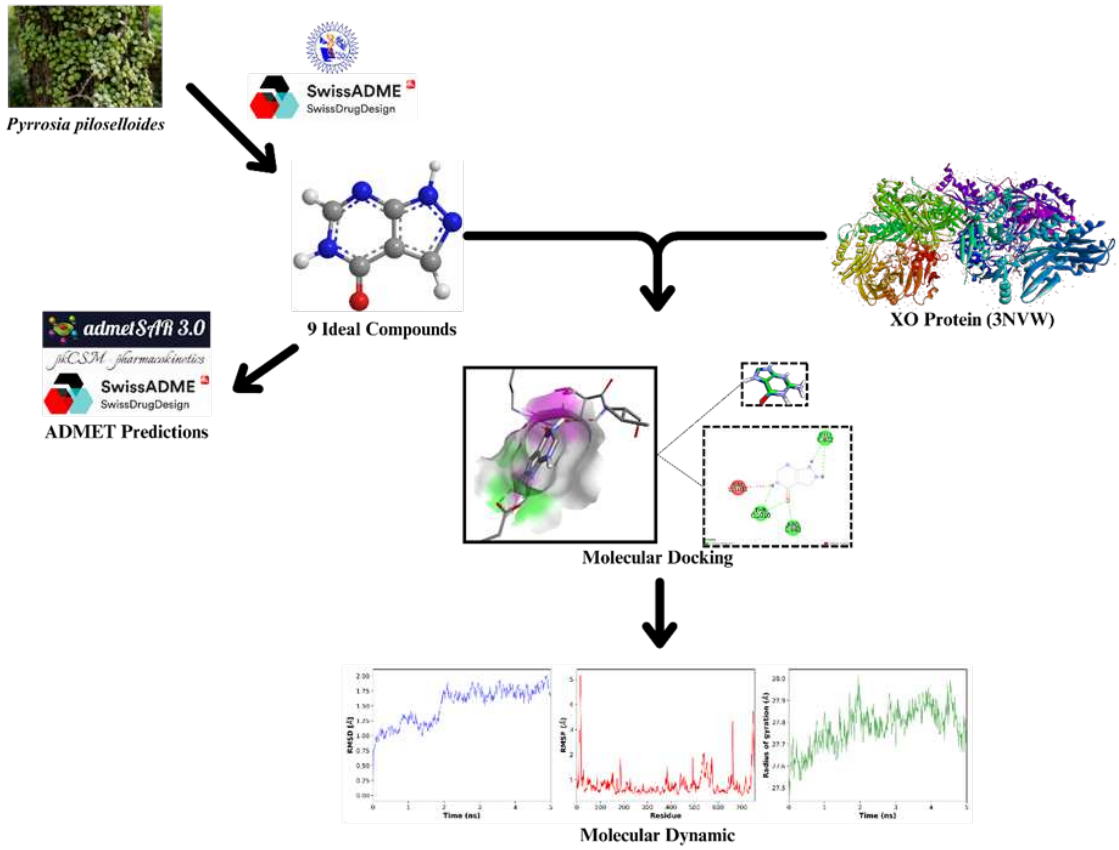

Figure 1. Workflow of schematic representation of the research

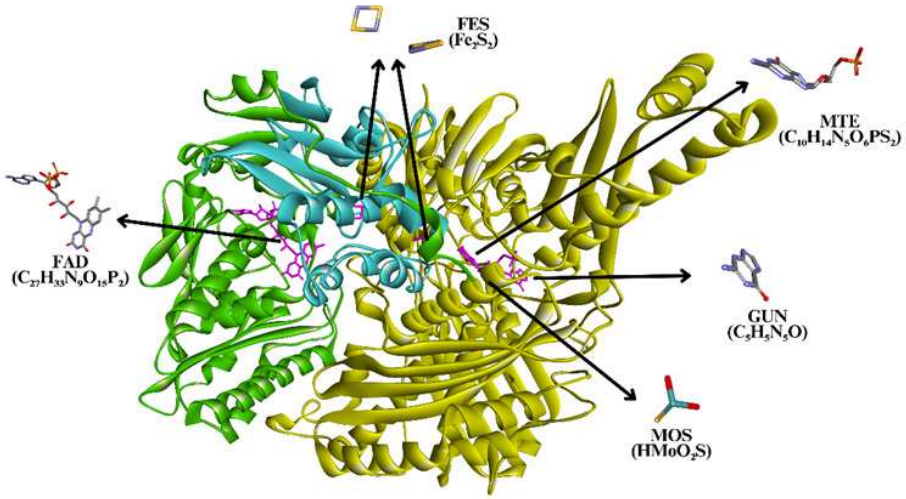

Figure 2. The XO protein complex with its native ligand. Chain A, chain B, and chain C are colored in light blue, green, and yellow, respectively.

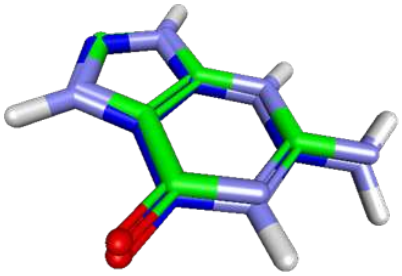

Figure 3. Overlapping between the co-crystal ligand (green) and the re-docked ligand (blue) with an RMSD value of 0.27 Å.

 ISSN:2527-7322 | e-ISSN: 2614-0020

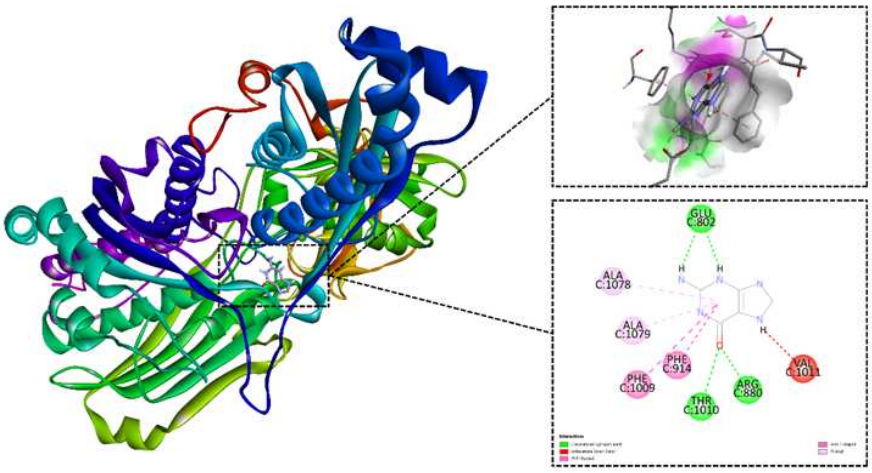

Figure 4. 2D and 3D Visualization of the Native Ligand (Guanine) Using BIOVIA Discovery Studio

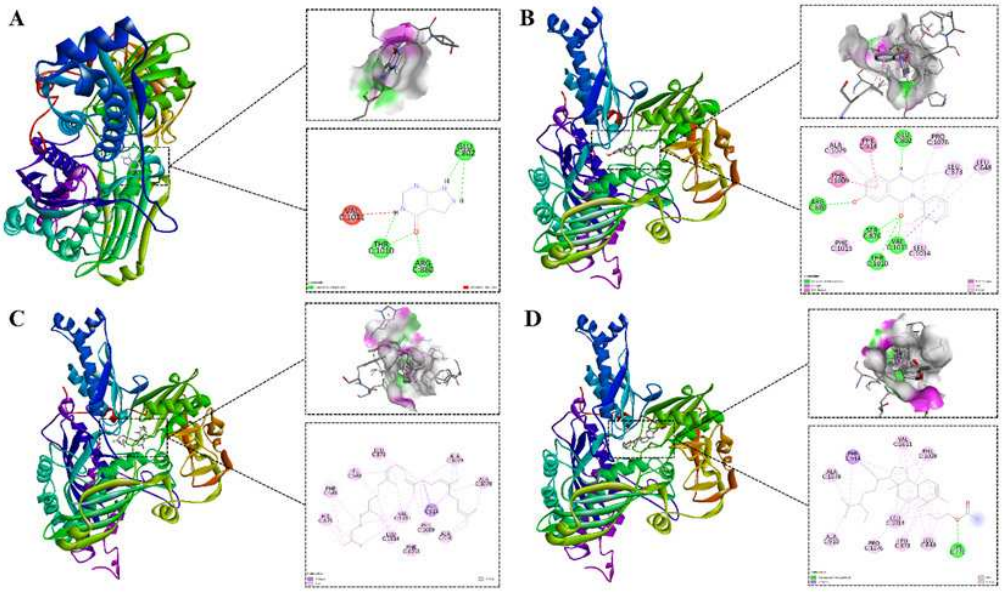

Figure 5. Results from the Best Ligands A = Allopurinol (Control), B = 6-Hydroxymethaqualone, C = 2,6,10,14,18,22-Tetracosahexaene, D = β-Sitosterol Acetate

ISSN:2527-7322 | e-ISSN: 2614-0020

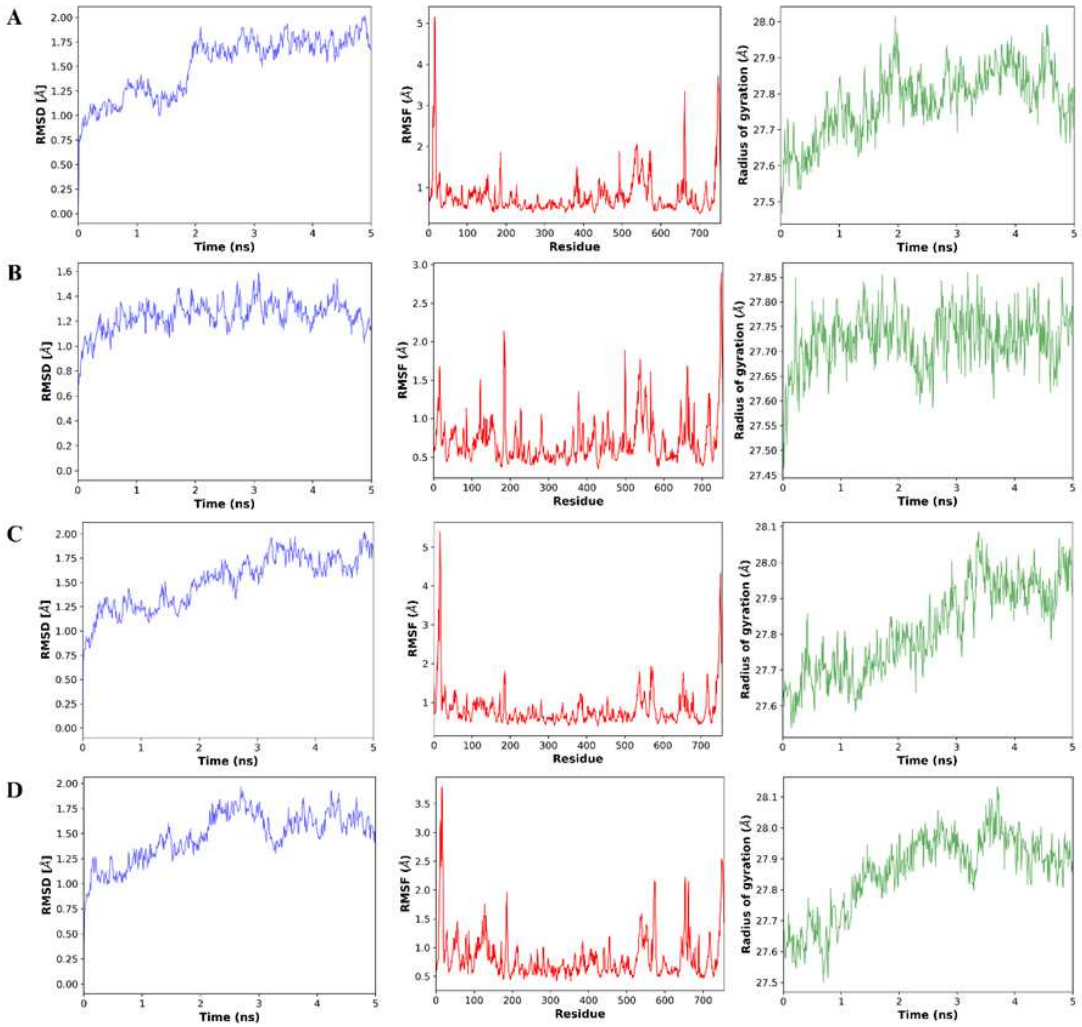

Figure 6. Molecular Dynamics Simulation Result A = Allopurinol , B = 6-Hydroxymethaqualone, C = 2,6,10,14,18,22-Tetracosahexaene, D = β-Sitosterol Acetate